

# Tensor-based techniques for fast discretization and solution of 3D elliptic equations with random coefficients

Venera Khoromskaia <sup>\*</sup>      Boris N. Khoromskij <sup>†</sup>

## Abstract

In this paper, we propose and analyze the numerical algorithms for fast solution of periodic elliptic problems in random media in  $\mathbb{R}^d$ ,  $d = 2, 3$ . We consider the stochastic realizations using checkerboard configuration of the equation coefficients built on a large  $L \times L \times L$  lattice, where  $L$  is the size of representative volume elements. The Kronecker tensor product scheme is introduced for fast generation of the stiffness matrix for FDM discretization on a tensor grid. We describe tensor techniques for the construction of the low Kronecker rank spectrally equivalent preconditioner in periodic setting to be used in the framework of PCG iteration. In our construction the diagonal matrix of the discrete Laplacian inverse represented in the Fourier basis is reshaped into a 3D tensor, which is then approximated by a low-rank canonical tensor, calculated by the multigrid Tucker-to-canonical tensor transform. The FDM discretization scheme on a tensor grid is described in detail, and the computational characteristics in terms of  $L$  for the 3D Matlab implementation of the PCG iteration are illustrated. The present work continues the developments in [22], where the numerical primer to study the asymptotic convergence rate vs.  $L$  for the homogenized matrix for 2D elliptic PDEs with random coefficients was investigated numerically. The presented elliptic problem solver can be applied for calculation of long sequences of stochastic realizations in numerical analysis of 3D stochastic homogenization problems for ergodic processes, for solving 3D quasi-periodic geometric homogenization problems, as well as in the numerical simulation of dynamical many body interaction processes and multi-particle electrostatics.

*Key words:* 3D elliptic problem solver, PDE with random coefficients, PCG iteration, low-rank tensor product approximation, Kronecker product, stochastic homogenization.

*AMS Subject Classification:* 65F30, 65F50, 65N35, 65F10

## 1 Introduction

Stochastic homogenization methods provide means for calculating the average characteristics of the structural and geometric properties of random composites. The numerical

---

<sup>\*</sup>Max-Planck-Institute for Mathematics in the Sciences, Inselstr. 22-26, D-04103 Leipzig, Germany (vekh@mis.mpg.de).

<sup>†</sup>Max-Planck-Institute for Mathematics in the Sciences, Inselstr. 22-26, D-04103 Leipzig, Germany (bokh@mis.mpg.de).

schemes for solving elliptic partial differential equations (PDEs) with random input in the form of stochastic/parametric elliptic equations have been intensively discussed in the literature [12, 2, 28, 30, 4, 5, 6, 11, 22, 31]. The theoretical analysis of quasi-periodic and stochastic/parametric problems can be found in [3, 29, 18, 10, 7] and in references therein. The rank structured tensor methods for quasi-periodic geometric homogenization methods and for the elliptic equations with highly oscillating coefficients were considered in [27, 20]. Data sparse and tensor methods for stochastic/parametric elliptic problems have been considered in [26, 28, 25, 33, 8, 9].

The main computational challenge in stochastic homogenization techniques is that the exhausting of the important information from the stochastic PDE (say, homogenized coefficient matrix or solution, and other important quantities of the stochastic process) requires a huge number of realizations, i.e. solving the target PDE many times for different stochastic input. In this respect, the valuable 3D stochastic simulations presuppose the strong requirements to the numerical efficiency of the chosen 3D elliptic problem solver.

This paper continues the development of efficient algorithms initiated by a numerical primer in [22] for fast solution of the 2D elliptic PDEs in random media, where the computational scheme for stochastic realizations using the general overlapping-type coefficient profile has been developed. The numerical study in [22] confirmed the theoretical convergence rate for the homogenized coefficients matrix in the size of representative volume element (RVE), presented in [13, 14, 16, 15]. Recall that the algorithms described in [22] are capable for 2D calculations with the number of realizations limited by the order of  $M = 10^5$ , implemented for coefficient configuration built on  $L \times L$  lattices with the RVE size  $L$  up to 128. However, the 3D calculations by using a general overlapping-type profile for generation of random coefficients seem to be prohibitive for the large number of coefficient realizations over  $L \times L \times L$  lattice structures.

In this paper, we describe the numerical scheme for discretization and solution of the  $d$ -dimensional stochastic homogenization problems for  $d = 2, 3$ , which employs the realizations over a checkerboard type configuration of the stochastic coefficient on the  $L \times L$  or  $L \times L \times L$  lattice, respectively. In 3D case, we use the product piecewise linear finite elements on the  $n \times n \times n$  Cartesian grids with  $n = n_0 L$ ,  $n_0 = 4, 8, 16, \dots$ , assuming that the jumps in the equation coefficient are resolved by non-overlapping square subdomains (unit cells). We introduce a tensor-based scheme for fast generation of the stiffness matrix for both 2D and 3D problems by using the Kronecker product construction for assembling of the FEM stiffness matrix and for the design of the rank-structured preconditioner. In the 3D case, we construct the spectrally equivalent preconditioner by employing the explicit representation (approximation) of the 3D periodic Laplacian operator inverse in the Fourier basis in a form of a short sum of the three-fold Kronecker products of  $n \times n$  matrices, similar to [17] where the Laplacian with Dirichlet boundary conditions was considered. Algorithmically, in our construction the diagonal matrix of the discrete Laplacian inverse represented in the Fourier basis is reshaped into a 3D tensor, which is then approximated by a low-rank canonical tensor, see Lemma 4.2. This approximation is calculated by using the multigrid Tucker-to-canonical tensor transform introduced in [23, 21].

The presented numerical scheme with the checkerboard type coefficients in 2D leads to a much faster method as compared with that for overlapping coefficients [22]. This allows

us to perform computations with RVE size  $L$  up to  $L = 512$  for 2D problems and for the number of realizations of the order of  $2^{15}$ . For 3D case the large number realizations,  $M$ , for RVE size up to  $L = 32, 64$ , discretized on  $n \times n \times n$  grids  $n = n_0 L$  can be calculated. The proposed tensor-based numerical techniques enable computations of the descriptive series of stochastic realizations for 2D and 3D problems in a wide range of the RVE size  $L$ , using MATLAB on a moderate computer cluster.

The proposed elliptic problem solver can be applied for the numerical analysis of 3D stochastic homogenization problems for ergodic processes with variable contrast in random coefficients, for solving numerically stochastic elliptic PDEs in random heterogeneous materials in  $\mathbb{R}^3$ , for fast solution of quasi-periodic (multi-scale) geometric homogenization problems for elliptic equations, in the computer simulation of dynamical many body interaction processes and multi-particle electrostatics, as well as for numerical analysis of optimal control problems in random media.

The rest of the paper is organized as follows. In Section 2, we describe the problem setting and specify the particular schemes for random generation of stochastic coefficients. Section 3 presents the main computational approach, where §3.1 describes the discretization scheme, §3.2 outlines the matrix generation by using Kronecker product sums and §3.3 sketches the method for fast matrix assembling of the stochastic part. Section 4 describes the construction of the efficient low Kronecker-rank spectrally close preconditioner in the PCG iteration for solving elliptic problems with variable coefficients arising for stochastic realizations with fixed value of RVE size,  $L$ , and the univariate grid size  $n$ . Section 5 presents the results of numerical experiments demonstrating the asymptotic complexity and timing of the Matlab implementation. In the spirit of [22], we also verify numerically the standard estimates on the asymptotic convergence rate for the simple average (standard deviation) of the homogenized coefficient matrix for 2D and 3D stochastic simulations with the checkerboard-type realization of coefficients.

## 2 General problem setting

For given  $f \in L^2(\Omega)$  such that  $\int_{\Omega} f(x) dx = 0$ , we consider the model elliptic boundary value problems on  $\Omega := [0, 1]^d$ , for  $d = 2, 3$ ,

$$\mathcal{A}\varphi := -\nabla \cdot \mathbb{A}(x)\nabla\varphi = f(x), \quad x = (x_1, \dots, x_d) \in \Omega, \quad (2.1)$$

endorsed with periodic boundary conditions on  $\Gamma = \partial\Omega$ . The diagonal  $d \times d$  coefficient matrix  $\mathbb{A}(x)$  is defined by

$$\mathbb{A}(x) = a(x)I_{d \times d}, \quad x \in \Omega,$$

where the scalar piecewise constant function  $a(x) > 0$  is generated randomly for every stochastic realization defined by the size  $L$  of RVE, such that it has many jumps in  $\Omega$ , see Figure 2.1 for the example in 2D case. There are many computational approaches for solving elliptic PDEs with random input, see [2, 6, 31, 22] and references therein. In particular, in [22] the fast elliptic problem solver in 2D case was applied to study numerically the convergence properties of the stochastic homogenization techniques, providing means to substitute the stochastic coefficient  $\mathbb{A}(x)$  by its simple homogenized version  $\bar{\mathbb{A}}_L \in \mathbb{R}^{2 \times 2}$ ,

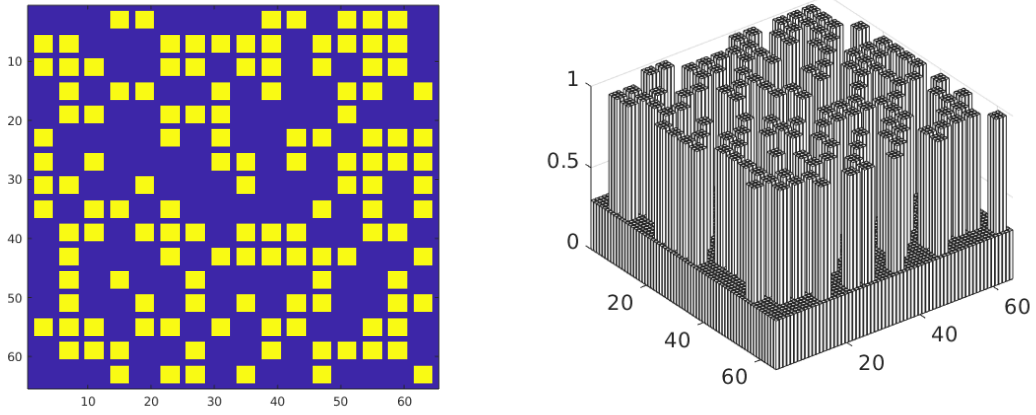


Figure 2.1: Example of stochastic realization of coefficient for  $L \times L$  lattice with  $L = 16$  with  $\lambda = 0.2$  and fixed contrast parameter  $\beta = 0.8$ .

such that for large values of RVE size  $L$  the average quantities over the long sequence of stochastic realizations will be very close to its homogenized version.

In this paper, we describe the new discretization and solution scheme for solving the  $d$ -dimensional problems with checkerboard type of random coefficients configuration  $\mathbb{A}(x)$  for  $d = 2, 3$ . We consider the sequence of  $M$  stochastic realizations specifying the variable part in the  $d \times d$  coefficient matrix  $\widehat{\mathbb{A}}_m(x)$ ,  $m = 1, \dots, M$ . For ease of exposition, we discuss the 3D problems,  $d = 3$ , and first, consider the case of constant scaling parameter  $\lambda$ . Fixed coefficient  $\widehat{\mathbb{A}}_m(x)$  and the scaling parameter  $0 < \lambda \leq 1$ , we solve the periodic elliptic problems in  $\Omega = [0, 1]^3$ ,

$$\mathcal{A}_m \phi := -\nabla \cdot \mathbb{A}_m(x) \nabla \phi = f(x), \quad x = (x_1, \dots, x_d) \in \Omega, \quad (2.2)$$

where the matrix-valued equation coefficient is specified by

$$\mathbb{A}_m(x) = \lambda I_{d \times d} + \beta \widehat{\mathbb{A}}_m(x) = a_m(x) I_{d \times d},$$

with  $\beta = 1 - \lambda$ , and the diagonal entry in  $\mathbb{A}_m(x)$  is defined by

$$a_m(x) = \lambda + \beta \widehat{a}_m(x). \quad (2.3)$$

Notice that in the application to numerical estimation of the homogenized matrix, see [22], the triple of elliptic equation has to be solved for every stochastic realization. Specifically, for  $i = 1, 2, 3$  the periodic elliptic problems in  $\Omega = [0, 1]^3$ ,

$$-\lambda \Delta \Phi_i - \beta \nabla \cdot \widehat{\mathbb{A}}_m(\cdot) (\mathbf{e}_i + \nabla \phi_i) = 0, \quad (2.4)$$

where  $\beta = 1 - \lambda$ , and the unit vectors  $\mathbf{e}_i$ ,  $i = 1, 2, 3$ , are given by

$$\mathbf{e}_1 = (1, 0, 0)^T, \quad \mathbf{e}_2 = (0, 1, 0)^T, \quad \mathbf{e}_3 = (0, 0, 1)^T.$$

The right-hand side in (2.2), rewritten in the canonical form (2.1), is represented by

$$f_i(x) = \beta \nabla \cdot \widehat{\mathbb{A}}_m(x) \mathbf{e}_i,$$

where the diagonal coefficient is defined in terms of the scalar function  $\widehat{a}_m(x)$ ,  $\widehat{\mathbb{A}}_m(x) = \widehat{a}_m(x) I_{d \times d}$ . Hence, we arrive at the representations for the right-hand sides

$$f_1(x) = \beta \frac{\partial \widehat{a}_m(x)}{\partial x_1}, \quad f_2(x) = \beta \frac{\partial \widehat{a}_m(x)}{\partial x_2}, \quad f_3(x) = \beta \frac{\partial \widehat{a}_m(x)}{\partial x_3}. \quad (2.5)$$

Figure 2.1 shows an example of stochastic realizations, which specify the locations of jumps in the equation coefficient  $a(x)$  in 2D case for  $L = 16$ .

In the previous simple model, we determine randomly the positions of jumps in the coefficients and use the constant length for the stochastic inclusions  $\beta = 1 - \lambda$ , which we call by the *contrast constant*. Our scheme also applies to the case of varying contrast constant  $\beta = \mu(x)$  that may vary in the interval  $\beta \in [0, \beta_0]$ ,  $\beta_0 = 1 - \lambda$ , randomly for each realization. Figures 2.2 and 2.3 illustrate the stochastic realizations of coefficients with two contrast parameters  $\beta_1 = 0.3$  and  $\beta_2 = 0.6$ , which are randomly distributed or have layer type structure.

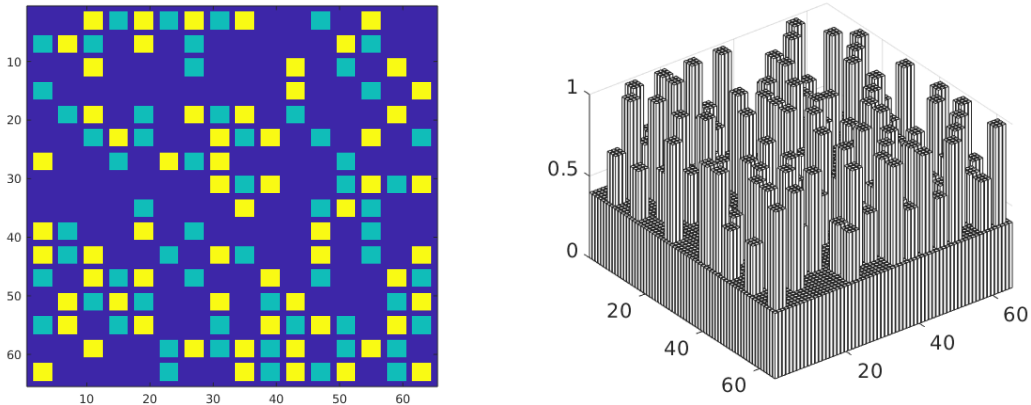


Figure 2.2: Example of stochastic realization of coefficient for  $L \times L$  lattice with  $L = 16$  with two contrast parameters  $\beta_1 = 0.3$  and  $\beta_2 = 0.6$ .

We are interested in the construction of fast numerical solution of the equation (2.4) with coefficients  $\mathbb{A}(x)$ , generated in the course of stochastic realizations. In this problem setting the bottleneck task is fast generation of the (large) FEM stiffness matrix in a sparse format, see [22], which should be re-calculated many thousands times for long sequences of stochastic realizations. Here the computational challenges are twofold:

- (A) Fine  $n \times n \times n$ -grids required for the resolution of coefficients on large  $L \times L \times L$  lattice.
- (B) Large number of stochastic realizations  $M$  of the order of  $10^4 - 10^5$  that are necessary for reliable estimation of desired stochastic quantities.

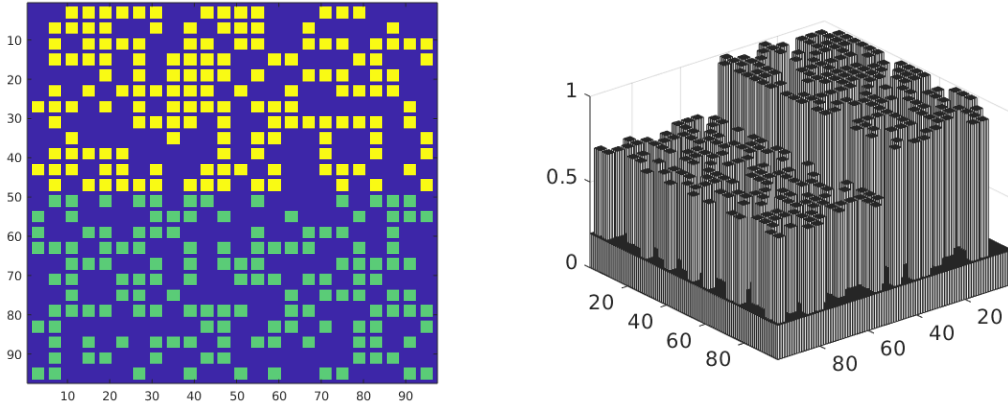


Figure 2.3: Example of stochastic realization of coefficient for  $L \times L$  lattice with  $L = 24$  with layer-type contrast parameters  $\beta = 0.6$  and  $\beta = 0.3$ .

In item (A) the construction of new FEM discretization and then generation of large stiffness matrix in data sparse format is required for every stochastic realization. Item (B) requires the fast iterative solver for the arising linear systems of equations, which should be robust with respect to the main model parameters  $L$ ,  $N = n^d$ , and the random equation coefficients. Our techniques suggest the effective approach for solving both problems (A) and (B).

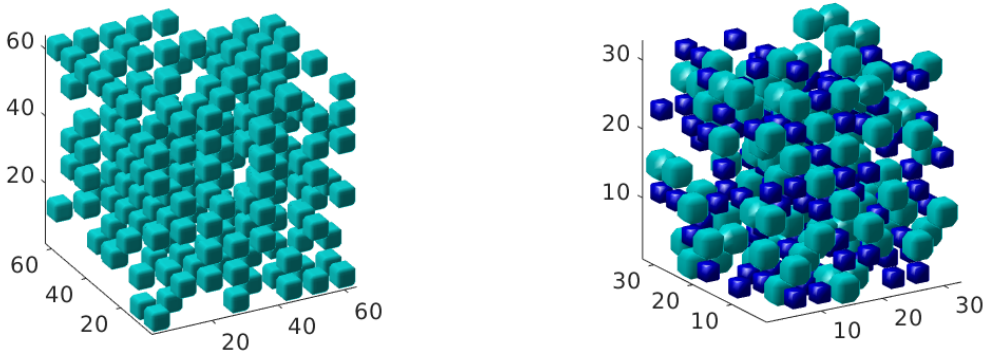


Figure 2.4: Example of 3D stochastic coefficient on  $L \times L \times L$  lattice with  $L = 8$  with fixed contrast  $\lambda$  (left), and two randomly distributed contrast parameters (right).

Figure 2.4 illustrates the configuration of the matrix coefficient visualized for an example of 3D realizations on the  $L \times L \times L$  lattice, with  $L = 8$ , The number of inclusions is about  $\frac{1}{2}L^3$ .

In what follows, we describe both fast and memory-efficient discretization and solution method for the class of stochastic PDEs specified above, which allows the reliable numerical estimate of the mean (homogenized) constant coefficient in the system (2.4) for  $d = 2, 3$  for rather large value of RVE  $L$  and various model parameters at the limit

of large  $M \rightarrow \infty$ , see [14, 15, 22]. This approach also allows to effectively estimate the average solution of the 3D stochastic PDE (2.1) with the given right-hand side  $f(x)$  by using the precomputed homogenized coefficient matrix.

### 3 Computational scheme for the stochastic average

#### 3.1 Galerkin FEM discretization scheme

The discretization scheme for the  $d$ -dimensional problem is constructed by FEM on tensor grid in  $\Omega \in \mathbb{R}^d$  similar to the 2D case described in [22]. We consider the RVE approximation specified by the checkerboard-type realizations of the random coefficient field on the  $L^{\otimes d}$  tensor product lattice<sup>1</sup>. This lattice is composed of  $L^d$  unit cells  $G_s$  such that

$$\Omega = \bigcup_{s=1}^{L^d} G_s.$$

In 2D case the FEM discretization and the construction of the Galerkin matrix can be viewed as a special case of the more general scheme in [22] based on the “overlapping” type random realizations of the coefficient field.

Given the number  $n_0 = 2^{p_0}$  with  $p_0 = 2, 3, 4, \dots$ , of the grid intervals specifying the size a unit cell, we introduce the uniform  $n_1^{\otimes d}$  rectangular grid  $\Omega_h$  in  $\Omega = [0, 1]^d$  with the grid size  $h = \frac{1}{n_1-1}$ , such that  $n_1 = n_0 L + 1$ , i.e.,  $h = \frac{1}{n_0 L}$ . We assume that the “unit cell”  $G_s$ ,  $s = 1, \dots, L^d$ , includes the square “unit sub-cell”  $S_s \subseteq G_s$  of size  $(\frac{2\alpha}{L})^{\otimes d}$  (that is  $\frac{2\alpha}{L} \times \frac{2\alpha}{L} \times \frac{2\alpha}{L}$  for  $d = 3$ ) which adjusts the square grid  $\Omega_h$ , such that the center  $c_s$  of  $S_s$  is located at the center of  $G_s$ . The sub-cell  $S_s$  denotes the region where the stochastic realization is allowed to generate the jumping coefficient. The number of unit cells  $K \leq L^d$  where the coefficient is perturbed varies for different stochastic realizations. The overlap factor  $0 < \alpha \leq \frac{2^{p_0-1}}{n_0}$  may take values  $\alpha \in \{\frac{1}{n_0}, \frac{2}{n_0}, \dots, \frac{2^{p_0-1}}{n_0}\}$  depending on the choice of  $p_0$ . In this construction the univariate size of the unit sub-cell  $S_s$  varies as

$$\frac{2\alpha}{L} = \frac{2\alpha n_0}{n_0 L} = kh, \quad \text{with} \quad k = 2, 4, \dots, n_0.$$

In the presented numerical examples we normally use the overlap constant  $\alpha = 1/4$  or  $\alpha = 1/2$ . For  $\alpha = 1/2$ , the maximal size of the unit sub-cell is given by  $(1/L)^{\otimes d}$ , which contains  $n_0 + 1$  grid points in each spacial direction leading to  $n_1^{\otimes d}$  rectangular grid with  $n_1 = n_0 L + 1$ .

Fixed  $L$ , the FEM discretization of the elliptic PDE in (2.2) can be constructed, in general, on a sequence of dyadic refined grids by choosing  $p_0 = 2, 3, \dots$ , so that the increase of the parameter  $p_0$  improves the accuracy of FEM approximation.

Given a finite dimensional space  $X \subset H^1(\Omega)$  of tensor product piecewise linear finite elements  $X = \text{span}\{\psi_\mu(x)\}$  associated with the grid  $\Omega_h$ , with  $\mu = 1, \dots, N_d$ ,  $N_d = n_1^d$ , incorporating periodic boundary conditions, we are looking for the traditional FEM Galerkin approximation of the exact solution in the form

$$\phi(x) \approx \phi_X(x) = \sum_{\mu=1}^{N_d} u_\mu \psi_\mu(x) \in X,$$

---

<sup>1</sup>That is  $L \times L$  lattice for  $d = 2$ , and  $L \times L \times L$  lattice for  $d = 3$ .

where  $\mathbf{u} = (u_1, \dots, u_{N_d})^T \in \mathbb{R}^{N_d}$  denotes the unknown coefficients vector. Fixed realization of the coefficient  $a^{(m)}(x)$ , we define the Galerkin-FEM discretization in  $X$  of the variational formulation of equation (2.2) by

$$A\mathbf{u} = \mathbf{f}, \quad A = [a_{\mu\nu}] \in \mathbb{R}^{N_d \times N_d}, \quad \mathbf{f} = [f_\mu] \in \mathbb{R}^{N_d}, \quad (3.1)$$

where the Galerkin-FEM stiffness matrix  $A$  generated by the equation coefficient  $\mathbb{A}^{(m)}(x)$  is calculated by using the associated bilinear form

$$a_{\mu\nu} = \langle \mathcal{A}\psi_\mu, \psi_\nu \rangle = \int_{\Omega} (\lambda \nabla \psi_\mu \cdot \nabla \psi_\nu + \beta a^{(m)}(x) \nabla \psi_\mu \cdot \nabla \psi_\nu) dx, \quad (3.2)$$

and  $f_\mu = \langle f, \psi_\mu \rangle$ .

In specific application to numerical estimation of the homogenized coefficient matrix the corresponding right-hand side is defined

$$f_{\mu,i} = \langle f, \psi_\mu \rangle = \beta \int_{\Omega} \nabla \cdot \widehat{a}^{(m)}(x) \mathbf{e}_i \psi_\mu dx = -\beta \int_{\Omega} \widehat{a}^{(m)}(x) \frac{\partial \psi_\mu}{\partial x_i} dx, \quad i = 1, 2, \dots, d. \quad (3.3)$$

Corresponding to (2.3) and (3.2), we represent the stiffness matrix  $A$  in the additive form

$$A = \lambda A_{\Delta} + \beta \widehat{A}_s, \quad (3.4)$$

where  $A_{\Delta}$  represents the  $N_d \times N_d$  FEM Laplacian matrix in periodic setting that has the standard  $d$ -term Kronecker product form. Here matrix  $\widehat{A}_s$  provides the FEM approximation to the "stochastic part" in the elliptic operator corresponding to the coefficient  $\widehat{a}^{(n)}(x)$ , see (2.3). The latter is determined by the sequence of random coefficient distributions in the course of stochastic realizations, numbered by  $m = 1, \dots, M$ .

In the case of complicated jumping coefficients the stiffness matrix generation in the elliptic FEM usually constitutes the dominating part of the overall solution cost. The asymptotic convergence of the stochastic homogenization process presupposes that the equation (3.1) has to be solved many hundred or even thousand times, so that for every realization one has to update the stiffness matrix  $A$  and the right-hand side  $\mathbf{f}$ .

Our discretization scheme computes all matrix entries at a low cost by assembling the local Kronecker products of sparse matrices obtained by representation of  $\widehat{a}^{(m)}(x)$  as a sum of separable functions. This allows to store the resultant stiffness matrix in the sparse matrix format. Such a construction only includes the pre-computing of small tri-diagonal matrices representing 1D elliptic operators with jumping coefficients in periodic setting. In the following sections, we shall describe the efficient construction of the "stochastic" term  $\widehat{A}_s$  to be updated for every realization.

### 3.2 Matrix generation by using Kronecker product sums

To enhance the time consuming matrix assembling process we apply the FEM Galerkin discretization (3.2) of equation (2.2) by means of the tensor-product piecewise linear finite elements

$$\{\psi_{\boldsymbol{\mu}}(x) := \psi_{\mu_1}(x_1) \cdots \psi_{\mu_d}(x_d)\}, \quad \boldsymbol{\mu} = (\mu_1, \dots, \mu_d), \quad \mu_\ell \in \mathcal{I}_\ell = \{1, \dots, n_\ell\},$$



for  $\ell = 1, \dots, d$ , where  $\psi_{\mu_\ell}(x_\ell)$  are the univariate piecewise linear hat functions. Notice that the univariate grid size  $n_\ell$  is of the order of  $n_\ell = O(1/\epsilon)$ , where the small homogenization parameter is given by  $\epsilon \approx 1/(n_0 L)$ , designating the total problem size

$$N_d = n_1 n_2 \cdots n_d = O(1/\epsilon^d).$$

The  $N_d \times N_d$  stiffness matrix is constructed by the standard mapping of the multi-index  $\boldsymbol{\mu}$  into the long univariate index  $1 \leq \mu \leq N_d$  for the active degrees of freedom in periodic setting. For instance, we use the so-called big-endian convention for  $d = 3$  and  $d = 2$

$$\boldsymbol{\mu} \mapsto \mu := \mu_3 + (\mu_2 - 1)n_3 + (\mu_1 - 1)n_2 n_3, \quad \boldsymbol{\mu} \mapsto \mu := \mu_2 + (\mu_1 - 1)n_2,$$

respectively. We first consider the case  $d = 2$  in more detail.

We calculate the stiffness matrix by assembling of the local Kronecker product terms by using representation of the ‘‘stochastic part’’ in the coefficient  $\widehat{a}^{(m)}(x)$  as an  $R$ -term sum of separable functions. This leads to the linear system of equations

$$\mathbf{A}\mathbf{u} = \mathbf{f}, \tag{3.5}$$

constructed for the general  $R$ -term separable coefficient  $a(x_1, x_2)$  with  $R \geq 1$ .

By simple algebraic transformations (e.g. by lumping of the mass matrices) the matrix  $A$  can be represented in the form (without loss of approximation order)

$$A \mapsto A = A_1 \otimes D_2 + D_1 \otimes A_2, \tag{3.6}$$

where  $D_1, D_2$  are the diagonal matrices with positive entries, and  $\otimes$  means the Kronecker product of matrices, see the discussion in [22]. This representation applies, in particular, to the periodic Laplacian. For example, in the case of anisotropic Laplacian the representation in (3.6) can be further simplified to

$$A \mapsto B = \alpha_2 A_1 \otimes I_2 + \alpha_1 I_1 \otimes A_2,$$

which will be used as a prototype preconditioner for solving the target linear system (3.5).

Taking into account the rectangular structure of the grid, we use the simple finite-difference (FD) scheme for the matrix representation of the Laplacian operator  $\Delta$ . The scaled discrete Laplacian incorporating periodic boundary conditions takes the form

$$A_\Delta = \Delta_{1,P} \otimes I_{n_2} + I_{n_1} \otimes \Delta_{2,P}, \tag{3.7}$$

where, say, in the variable  $x_1$  we have

$$\Delta_{1,P} = -\text{tridiag}\{1, -2, 1\} + P^{(1)} \in \mathbb{R}^{n_1 \times n_1},$$

such that the entries of the ‘‘periodization’’ matrix  $P^{(1)} \in \mathbb{R}^{n_1 \times n_1}$  are all zeros except

$$P_{1,n_1}^{(1)} = P_{n_1,1}^{(1)} = 1, \quad \text{and} \quad P_{1,1}^{(1)} = P_{n_1,n_1}^{(1)} = -1,$$

see (3.8), right. Here  $I_{n_1} \in \mathbb{R}^{n_1 \times n_1}$  is the identity matrix,  $\Delta_{1,P}$  and  $\Delta_{2,P}$  are the 1D finite difference Laplacians in variables  $x_1$  and  $x_2$ , respectively (endorsed with the Neumann

boundary conditions). We say that the Kronecker rank of the matrix  $A$  in (3.7) equals to 2,  $\text{rank}_{Kron}(A) = 2$ .

For the assembling of the stiffness we also need the 1D Laplacian with Neumann boundary conditions. To that end we notice that the  $n_1 \times n_1$  Laplacian matrices for the Neumann and periodic boundary conditions in the first 1D variable read as

$$\Delta_{1,N} = \begin{bmatrix} -1 & 1 & \cdots & 0 & 0 \\ 1 & -2 & \cdots & 0 & 0 \\ \vdots & \vdots & \ddots & \vdots & \vdots \\ 0 & 0 & \cdots & -2 & 1 \\ 0 & 0 & \cdots & 1 & -1 \end{bmatrix} \quad \text{and} \quad \Delta_{1,P} = \begin{bmatrix} -2 & 1 & \cdots & 0 & 1 \\ 1 & -2 & \cdots & 0 & 0 \\ \vdots & \vdots & \ddots & \vdots & \vdots \\ 0 & 0 & \cdots & -2 & 1 \\ 1 & 0 & \cdots & 1 & -2 \end{bmatrix}, \quad (3.8)$$

respectively.

In the  $d$ -dimensional setting we have the similar Kronecker rank- $d$  representations. For example, in the case  $d = 3$  the "periodic"  $N_d \times N_d$  Laplacian matrix  $A_\Delta$  takes a form

$$A_\Delta = A_{1,P} \otimes I_2 \otimes I_3 + I_1 \otimes A_{2,P} \otimes I_3 + I_1 \otimes I_2 \otimes A_{3,P}, \quad (3.9)$$

such that its Kronecker rank equals to 3, while for the arbitrary  $d \geq 3$ , we have  $\text{rank}_{Kron}(A) = d$ .

### 3.3 Fast matrix assembling for the stochastic part

The Kronecker form representation of the "stochastic" term in (3.2) further denoted by  $\widehat{A}_s$  is more involved. For the ease of exposition we, first, discuss the case  $d = 2$ , and assume that  $n_1 = n_2$ .

For given stochastically chosen distribution of non-overlapping cells  $S_k$ ,  $k = 1, \dots, K$ , where the constant coefficient is perturbed, we introduce the full covered grid domain  $\widehat{G} = \cup_{k=1}^K S_k \subset \Omega$  colored by black in Figure 2.1 and 5.1. We obtain a union of non-overlapping "covered" square cells  $S_k$ ,  $k = 1, \dots, K$ ,  $K \leq L^2$ , each of the grid-size  $\bar{n}_0 \times \bar{n}_0$ ,

$$\widehat{G} = \cup_{k=1}^K S_k, \quad S_k \subseteq G_k, \quad (3.10)$$

where the number  $K$  varies for different realizations. By construction, we have  $a(x) = 1$  for  $x \in \widehat{G}$  and  $a(x) = \lambda$  for  $x \in \Omega \setminus \widehat{G}$ . Here  $\bar{n}_0 = 2^p + 1$ , for some  $p = 1, 2, \dots, p_0$ , is fixed as above by the chosen overlap constant  $\alpha > 0$ , see §3.1. In this construction, the non-overlapping elementary cells  $S_k$  for different  $k$  are allowed to have the only common edges of size  $\bar{n}_0$ .

Notice that in the case of non-overlapping decomposition (3.10) the set of cells  $\{S_k\}$  may coincide with the initial set  $\{G_s\}$  that allows to maximize the size  $\bar{n}_0 \times \bar{n}_0$  of each  $S_k$ ,  $k = 1, \dots, L^2$ , to the largest possible, i.e. to  $\bar{n}_0 = n_0 + 1$ . We refer to [22] for the construction in the case of general overlapping coefficients.

To finalize the matrix generation procedure for  $\widehat{A}_s$ , we define the local  $\bar{n}_0 \times \bar{n}_0$  matrices representing the discrete Laplacian with Neumann boundary conditions,

$$\widehat{Q}_{\bar{n}_0} := \text{tridiag}\{1, -2, 1\} + \text{diag}\{1, 0, \dots, 0, 1\} \in \mathbb{R}^{\bar{n}_0 \times \bar{n}_0},$$

and the diagonal matrix

$$\widehat{I}_{\bar{n}_0} := \text{diag}\{1/2, 1, \dots, 1, 1/2\} \in \mathbb{R}^{\bar{n}_0 \times \bar{n}_0},$$

see the visualization in (3.8), left. Here, we may select  $\bar{n}_0 = 3, 5, \dots$  that corresponds to the choice  $p = 1, 2, \dots$ . In the case of  $\bar{n}_0 \times \bar{n}_0$  matrix with minimal size  $\bar{n}_0 = 3$ , both discrete Laplacians in (3.8) simplify to

$$\Delta_N = \begin{bmatrix} -1 & 1 & 0 \\ 1 & -2 & 1 \\ 0 & 1 & -1 \end{bmatrix} \quad \text{and} \quad \Delta_P = \begin{bmatrix} -2 & 1 & 1 \\ 1 & -2 & 1 \\ 1 & 1 & -2 \end{bmatrix}. \quad (3.11)$$

Let the subdomain  $S_k$  be supported by the index set  $I_k^{(1)} \times I_k^{(2)}$  of size  $\bar{n}_0 \times \bar{n}_0$  for  $k = 1, \dots, K$ . Introduce the block-diagonal matrices  $\overline{Q}_k \in \mathbb{R}^{n_1 \times n_1}$  and  $\overline{I}_k \in \mathbb{R}^{n_1 \times n_1}$  by inserting matrices  $\widehat{Q}_{\bar{n}_0}$  and  $\widehat{I}_{\bar{n}_0}$ , defined above, as diagonal blocks into  $n_1 \times n_1$  zero matrix in the positions  $I_k^{(1)} \times I_k^{(1)}$  and  $I_k^{(2)} \times I_k^{(2)}$ , respectively. Now the stiffness matrix  $\widehat{A}_s$  is represented in the form of a Kronecker product sum as follows,

$$\widehat{A}_s = \sum_{k=1}^K (\overline{Q}_k \otimes \overline{I}_k + \overline{I}_k \otimes \overline{Q}_k) + P^{(2)}, \quad (3.12)$$

where

$$P^{(2)} = P^{(1)} \otimes I_{n_1} + I_{n_1} \otimes P^{(1)} \in \mathbb{R}^{N_d \times N_d}$$

is the "periodization" matrix in 2D.

In a  $d$ -dimensional case the representation (3.12) generalizes to a sum of  $d$ -factor Kronecker products

$$\widehat{A}_s = \sum_{k=1}^K (\overline{Q}_k \otimes \overline{I}_k \otimes \dots \otimes \overline{I}_k + \dots + \overline{I}_k \otimes \dots \otimes \overline{I}_k \otimes \overline{Q}_k) + P^{(d)}, \quad (3.13)$$

where  $P^{(d)}$  is the "periodization" matrix in  $d$  dimensions, constructed as the  $d$ -term Kronecker sum similar to the case  $d = 2$ .

The Kronecker product form of (3.12) and (3.13) leads to the corresponding Kronecker sum representation for the total stiffness matrix  $A$ . This allows an efficient implementation of the matrix assembly and low storage request for the stiffness matrix preserving the Kronecker sparsity. In general, for 2D case the number  $K$  of elementary cells<sup>2</sup> does not exceed  $L^2$ , and it may coincides with  $L^2$  only in the case of non-overlapping decomposition  $\widehat{G} = \cup_{k=1}^{L^2} S_k$  with maximal size  $\bar{n}_0 = n_0 + 1$ , where different patches  $S_k$  are allowed to have joint pieces of boundary, but no overlapping area.

The technical assumption that all sub-cells  $S_k$  are supposed to be cell-centered is not essential for the presented construction. The approach also applies to the case of general location of  $S_k$  inside of the corresponding unit cell  $G_k$ .

For the above constructions, which apply to any dimension  $d$ , we are able to prove the following storage complexity and Kronecker rank estimates for the stiffness matrix  $A$ .

---

<sup>2</sup>For example, for cells of minimal size,  $\bar{n}_0 \times \bar{n}_0$  with  $\bar{n}_0 = 3$ , as in (3.11), we have  $K = O(n_1^2)$ .

**Lemma 3.1** *The storage size for the stiffness matrix  $A$  is bounded by*

$$\text{Stor}(A) \approx \text{Stor}(\widehat{A}_s) = O(d\bar{n}_0 K + dn_1), \quad K \leq L^d.$$

*In the general case  $d \geq 2$  the Kronecker rank of the matrix  $A$  is bounded by*

$$\text{rank}_{Kron}(A) \leq K \leq L^d.$$

*In the case of cell-centered locations of subdomains  $S_k$  (special case of geometric homogenization) there holds*

$$\text{rank}_{Kron}(A) \leq L^{d-1}.$$

*Proof.* The first two estimates directly follow from the construction. To justify the improved rank estimate in 2D case we notice that the  $K$ -term sum in (3.12) can be simplified as follows. Introduce the  $L$  horizontal grid strips  $\mathcal{S}_\ell$ ,  $\ell = 1, \dots, L$ , each of width  $n_0$  and agglomerate all the summands in (3.12) with  $S_k \subseteq \mathcal{S}_\ell$  into one matrix  $A_\ell$ . It can be seen that  $\text{rank}_{Kron}(A_\ell) = 1$ . Hence the equation

$$A = \sum_{\ell=1}^L A_\ell$$

proves the result for  $d = 2$ . The rank estimate in the case  $d \geq 3$  can be derived completely similar.  $\blacksquare$

The discretized equation (2.2) takes a form

$$A\mathbf{u} = \mathbf{f}, \tag{3.14}$$

where the FEM-Galerkin matrix  $A$  generated by the equation coefficient  $\mathbb{A}_n(x)$  is calculated as described above (see [22] for the case of overlapping decompositions).

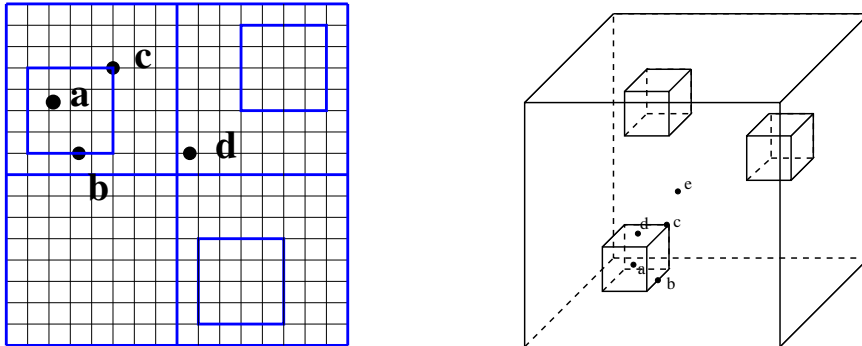


Figure 3.1: Accounting jumping coefficients at grid points (a), (b), (c) and (d) for the 2D problem depending on the location from the supports of the bump (left), and at points (a), (b), (c), (d) and (e) for the 3D problem (right).

Notice that in application to RVE approximation of the homogenized matrix one has to solve  $d$  linear systems of equations with different right-hand sides. The corresponding vector representation  $\mathbf{f}_i \in \mathbb{R}^N$ ,  $i = 1, \dots, d$ , of the right-hand side  $f_i(x)$  is computed by

scalar multiplication of  $f_i(x)$  with the corresponding Galerkin basis function and integration by parts, see (3.3).

Specifically, given the grid-point  $x_h \in \Omega_h$ , the corresponding value of the diagonal coefficient is defined by  $a_m(x_h)$ , see (2.3). In case  $d = 2$  the variable part  $\widehat{a}_m(x_h)$ , describing the jumping coefficient, is assigned by 1 for interior points in  $\widehat{G}$ , by  $1/2$  for interface points (the angle equals to  $\pi/2$ ), and by  $1/4$  for the "exterior" corner of  $\widehat{G}$  (the angle equals to  $\pi/4$ ), see points (d), (b), (c) and (a) in Figure 3.1 (left), respectively. Figure 3.1 (left) corresponds to  $L = 2$ , the discretization parameter  $n_0 = 8$  and the periodic completion of the geometry.

The corresponding illustration for the 3D case is presented in Figure 3.1 (right). In case of large number of representative volume elements,  $L$ , one observes the complicated interface defining the strongly jumping coefficients.

### 3.4 The RVE approximation of homogenized matrix

For given size of the RVE,  $L$ , we consider the sequence of problems for stochastic realizations specifying the variable part in the  $d \times d$  coefficient matrix  $\widehat{\mathbb{A}}^{(m)}(x)$ ,  $m = 1, \dots, M$ ,

$$-\lambda \Delta \phi_i - \beta \nabla \cdot \widehat{\mathbb{A}}^{(m)}(\cdot)(\mathbf{e}_i + \nabla \phi_i) = 0, \quad (3.15)$$

for  $i = 1, \dots, d$ .

Fixed  $L$  and the particular realization  $\mathbb{A}_L^{(m)}(x) = \lambda I + \beta \widehat{\mathbb{A}}^{(m)}(x)$ , the averaged coefficient matrix  $\bar{\mathbb{A}}_L^{(m)} = [\bar{a}_{L,ij}^{(m)}] \in \mathbb{R}^{d \times d}$ ,  $i, j = 1, \dots, d$ , with the constant entries is conventionally defined by the equation

$$\bar{\mathbb{A}}_L^{(m)} \mathbf{e}_i = \int_{\Omega} \mathbb{A}_L^{(m)}(x)(\mathbf{e}_i + \nabla \phi_i) dx, \quad (3.16)$$

which implies the representation for matrix elements

$$\bar{a}_{L,ij}^{(m)} \equiv \bar{a}_{ij}^{(m)} = \int_{\Omega} [(\lambda I_{d \times d} + \beta \widehat{\mathbb{A}}^{(m)}(x))(\mathbf{e}_i + \nabla \phi_i)]_j dx, \quad i, j = 1, \dots, d.$$

The latter leads to the entry-wise representation of the homogenized matrix  $\bar{\mathbb{A}}^{(m)} = [\bar{a}_{ij}^{(m)}]$ ,  $i, j = 1, \dots, d$ ,

$$\begin{aligned} \bar{a}_{ii}^{(m)} &= \int_{\Omega} a_n(x) \left( \frac{\partial \phi_i}{\partial x_i} + 1 \right) dx \quad i = 1, \dots, d, \\ \bar{a}_{ij}^{(m)} &= \int_{\Omega} a_n(x) \frac{\partial \phi_i}{\partial x_j} dx \quad i, j = 1, \dots, d, \quad i \neq j. \end{aligned} \quad (3.17)$$

Taking into account (2.3) and (2.5), we obtain the computationally convenient representation

$$\begin{aligned} \bar{a}_{ii}^{(m)} &= \lambda + \beta \int_{\Omega} \widehat{a}_m(x) dx - \beta \int_{\Omega} \frac{\partial \widehat{a}_m(x)}{\partial x_i} \phi_i dx \\ &= \lambda + \beta \int_{\Omega} \widehat{a}_m(x) dx - \int_{\Omega} f_i \phi_i dx, \quad i = 1, \dots, d, \\ \bar{a}_{ij}^{(m)} &= -\beta \int_{\Omega} \frac{\partial \widehat{a}_m(x)}{\partial x_j} \phi_i dx = - \int_{\Omega} f_j \phi_i dx, \quad i, j = 1, \dots, d, \quad i \neq j. \end{aligned} \quad (3.18)$$

The representation (3.18) ensures the symmetry of the homogenized matrix  $\bar{\mathbb{A}}^{(m)}$ , i.e.  $\bar{a}_{ij}^{(m)} = \bar{a}_{ji}^{(m)}$ , taking into account the equations (2.4), see [22], §4.2, for the detailed argument.

In numerical implementation, we apply the same variational scheme for calculation (by numerical integration) of  $\bar{\mathbb{A}}^{(m)}$  as for the FEM discretization of the operator and the right-hand side in the initial elliptic PDE, thus preserving the symmetry of the matrix  $\bar{\mathbb{A}}^{(m)}$  inherited from the initial variational formulation.

Furthermore, integrals over  $\Omega$  in (3.18), as they are written for the exact matrix entries  $\bar{a}_{ij}^{(m)}$ ,  $i, j = 1, \dots, d$ , are calculated (approximately) by using the discrete representation of integrand on the grid  $\Omega_h$ .

## 4 Construction of preconditioner for PCG iteration

### 4.1 Spectral equivalent preconditioner

Let the right-hand side in (2.1) satisfy  $\langle \mathbf{f}, \mathbf{1} \rangle = 0$ , then for a fixed realization  $n$ , the equation

$$A_m \mathbf{u} = (\lambda A_\Delta + \beta A_{s,m}) \mathbf{u} = \mathbf{f}, \quad (4.1)$$

where  $A_\Delta = \Delta_h$  is the periodic Laplacian, has the unique solution. We solve this equation by the preconditioned conjugate gradient (PCG) iteration with the preconditioner obtained as inverse of the (perturbed) periodic Laplacian

$$B_\Delta = \frac{1 + \lambda}{2} A_\Delta + \delta I,$$

where  $I$  is the  $N_d \times N_d$  identity matrix and  $\delta \geq 0$  is a small regularization parameter introduced for stability reasons in the case of direct inversion of  $B_\Delta$  (that is too costly in 3D case). In what follows, for 3D case, we set up  $\delta = 0$  and use the explicit low Kronecker rank approximation of the pseudo-inverse matrix  $B_\Delta^+$  as the preconditioner for solving the algebraic system of equations (4.1) on the subspace  $\langle \mathbf{u}, \mathbf{1} \rangle = 0$ . Notice that by the conventional definition we have  $B_\Delta^+ B_\Delta \mathbf{u} = \mathbf{u}$  for all  $\mathbf{u}$  such that  $\langle \mathbf{u}, \mathbf{1} \rangle = 0$ , while  $B_\Delta^+ \mathbf{1} = 0$ . Since the pre-factor  $\frac{1+\lambda}{2}$  does not effect the condition number of the preconditioned matrix, in the following discussion we set up it as 1.

It can be proven that the condition number of preconditioned matrix is uniformly bounded in  $n_1$  and  $L$ . The following Lemma proves the spectral equivalence of the preconditioner, see also [22].

**Lemma 4.1** *Given the matrix  $B_\Delta$  with  $\delta = 0$ , then for any stochastic realization the condition number of the preconditioned matrix  $B_\Delta^+ A_n$  on the kernel of the stiffness matrix  $A_n$ ,  $\langle \mathbf{u}, \mathbf{1} \rangle = 0$ , is uniformly bounded in  $n_1$ ,  $L$  and  $\alpha$ , such that*

$$\text{cond}\{B_\Delta^+ A_n\} \leq C \lambda^{-1}.$$

*Proof.* The particular bound on the condition number in terms of a parameter  $\lambda$  can be derived by introducing the average coefficient

$$a_0(x) = \frac{1}{2}(a^+(x) + a^-(x)),$$

where  $a^+(x)$  and  $a^-(x)$  are chosen as *majorants and minorants* of  $a_m(x)$  in (2.3), respectively. Indeed, the preconditioner  $B_0^+$  generated by the coefficient  $a_0(x) = \frac{1}{2}(a^+(x) + a^-(x))$  allows the condition number estimate

$$\text{cond}\{B_0^+ A_n\} \leq C \max \frac{1+q}{1-q}, \quad \text{with } q := \max(a^+(x) - a_0(x))/a_0(x) < 1$$

on the subspace  $\langle \mathbf{u}, 1 \rangle = 0$ . With the choice  $\delta = 0$ , the preconditioner  $B_\Delta^+$  corresponds to  $a^+(x) = 1$  and  $a^-(x) = \lambda$ , hence, we obtain  $a_0(x) = \frac{1+\lambda}{2}$  and the result follows.  $\blacksquare$

The PCG solver for the system of equations (3.14) with the pseudo-inverse of the discrete Laplacian as the preconditioner demonstrates robust convergence with the rate  $q < 1$  almost uniformly in the model and discretization parameters  $L, \lambda, \alpha$  and the grid size  $n_1$ .

Recall that the periodic Laplacian obeys the Kronecker rank- $d$  representation, that is the  $d$ -level circulant matrix, and, hence, it can be diagonalized by the Fourier transform. In particular, in the 2D case the periodic Laplacian takes form (3.7). In the case  $d = 3$ , the  $N_d \times N_d$  "periodic" Laplacian matrix  $A_\Delta$  is the three-term Kronecker sum (3.9) and similar for the  $d$ -term representation in the general case  $d \geq 3$ .

In the rest of this section, we discuss the main details of our reconditioned PCG scheme for periodic setting that relies on the low Kronecker rank approximation of the pseudo-inverse matrix  $B_\Delta^+$ . In this scheme the CG iteration applies to the preconditioned system of equations in (4.1) as follows

$$B_\Delta^+ A_n \mathbf{u} = B_\Delta^+ \mathbf{f}, \quad (4.2)$$

that is solved on the subspace  $\langle \mathbf{u}, 1 \rangle = 0$  due to periodic setting.

Notice that in the case of homogeneous Dirichlet problem such a scheme with the choice  $B_\Delta^{-1} = A_\Delta^{-1}$  was described in [17]. In §4.2 we modify this construction to the periodic setting.

## 4.2 Low Kronecker rank approximation of the preconditioner

The rank-structured preconditioner presented here for periodic setting is obtained by a modification of the construction described in [17] for the Dirichlet boundary conditions, see also [32] where the case of anisotropic Laplacian is considered.

In the periodic setting, the matrix  $A_\Delta$  can be diagonalized in the  $d$ -dimensional Fourier basis, which implies the factorization (for example, in 2D case)

$$\begin{aligned} A_\Delta &= (F_1^* \otimes F_2^*)(\Lambda_1 \otimes I_2)(F_1 \otimes F_2) + (F_1^* \otimes F_2^*)(I_1 \otimes \Lambda_2)(F_1 \otimes F_2) \\ &= (F_1^* \otimes F_2^*)\Lambda(F_1 \otimes F_2), \end{aligned} \quad (4.3)$$

with the diagonal matrix

$$\Lambda := \Lambda_1 \otimes I_2 + I_1 \otimes \Lambda_2 \in \mathbb{R}^{n_1^2 \times n_1^2}.$$

Furthermore, in 3D case we have

$$\begin{aligned} A_\Delta &= (F_1^* \otimes F_2^* \otimes F_3^*)(\Lambda_1 \otimes I_2 \otimes I_3)(F_1 \otimes F_2 \otimes F_3) \\ &\quad + (F_1^* \otimes F_2^* \otimes F_3^*)(I_1 \otimes \Lambda_2 \otimes I_3)(F_1 \otimes F_2 \otimes F_3) \\ &\quad + (F_1^* \otimes F_2^* \otimes F_3^*)(I_1 \otimes I_2 \otimes \Lambda_3)(F_1 \otimes F_2 \otimes F_3) \\ &= (F_1^* \otimes F_2^* \otimes F_3^*)\Lambda(F_1 \otimes F_2 \otimes F_3), \end{aligned} \quad (4.4)$$

with the diagonal matrix  $\Lambda$  given by

$$\Lambda := \Lambda_1 \otimes I_2 \otimes I_3 + I_1 \otimes \Lambda_2 \otimes I_3 + I_1 \otimes I_2 \otimes \Lambda_3 \in \mathbb{R}^{n_1^3 \times n_1^3}. \quad (4.5)$$

Here the  $n_1 \times n_1$  diagonal matrices  $\Lambda_\ell = \text{diag}\{F_\ell(\mathbf{p})\} \in \mathbb{R}^{n_1 \times n_1}$ ,  $\ell = 1, \dots, d$ , are defined by the Fourier transform  $F_\ell(\mathbf{p}) \in \mathbb{R}^{n_1}$  of the first column vector

$$\mathbf{p} = (2, -1, 0, \dots, 0, -1)^T \in \mathbb{R}^{n_1}$$

in the circulant matrix  $\Delta_P$  in (3.8), diagonalized by the Fourier transform

$$\Delta_P = F_\ell^* \text{diag}\{F_\ell(\mathbf{p})\} F_\ell = F_\ell^* \text{diag}\{\lambda_1, \dots, \lambda_{n_1}\} F_\ell. \quad (4.6)$$

Here  $\lambda_i = [F_\ell(\mathbf{p})]_i$ ,  $i = 1, \dots, n_1$ , denote the eigenvalues of the periodic Laplacian  $\Delta_P$ , such that  $\lambda_1 = 0$ . The latter property introduces the significant difference between the periodic case and the case of Dirichlet boundary conditions considered in [17].

The representations (4.3) and (4.4) give rise to the eigenvalue decomposition of  $A_\Delta$ . Therefore, for a function  $\mathcal{F}$  applied to the matrix  $A_\Delta$ , we arrive at

$$\mathcal{F}(A_\Delta) = (F_1^* \otimes F_2^*) \mathcal{F}(\Lambda) (F_1 \otimes F_2), \quad (4.7)$$

and

$$\mathcal{F}(A_\Delta) = (F_1^* \otimes F_2^* \otimes F_3^*) \mathcal{F}(\Lambda) (F_1 \otimes F_2 \otimes F_3), \quad (4.8)$$

for 2D and 3D cases, respectively. In our application we have to approximate the diagonal matrix  $\mathcal{F}(\Lambda) = \Lambda^{-1}$  in the case of periodic Laplacian, where  $A_\Delta$  has zero eigenvalue.

To construct the efficient preconditioner for the system matrix  $A_n$ , we are particularly interested in the low Kronecker rank approximation of the pseudo-inverse matrix  $A_\Delta^+$  that provides the spectrally close approximation to  $\mathcal{F}(A_n) = A_n^+$ . Since in the case of periodic boundary conditions the matrix  $A_n$  has zero eigenvalue corresponding to the constant vector, one has to consider the pseudo-inverse matrix  $A_\Delta^+$  instead of the standard inverse  $A_\Delta^{-1}$  that means the matrix  $\Lambda^+$  should be defined by setting the first element in  $\Lambda^{-1}$  to zero.

We discuss two different solution strategies for multiple solving the target algebraic system of linear equations in (4.1).

*The first approach* is based on the FFT diagonalization of pseudo-inverse preconditioning matrix  $A_\Delta^+$  by using the pseudo-inverse  $\Lambda^+$ . In this case the system matrix is stored in the standard sparse matrix format and the PCG solution process is performed in the exact matrix arithmetics.

*In the second approach*, we represent both the system matrix and preconditioner in the low Kronecker rank form and store both large matrices  $A_n$  and  $A_\Delta^+$  as a small set of thin Kronecker factor matrices which allows to implement the PCG iteration on the low parametric manifold of low-rank discretized functions.

Here we briefly discuss the second approach. In the 3D case, the elements of the core diagonal matrix  $\Lambda$  in (4.5) can be represented as a three-tensor

$$\mathbf{G} = [g(i_1, i_2, i_3)] \in \mathbb{R}^{n_1 \times n_2 \times n_3}, \quad i_\ell \in \{1, \dots, n_\ell\},$$



where

$$g(i, j, k) = \lambda_i + \lambda_j + \lambda_k,$$

implying that  $\mathbf{G}$  has the exact rank-3 decomposition. Here the periodicity conditions imply  $\lambda_1 = 0$  such that  $g(1, 1, 1) = 0$ . In the case  $d = 2$  we have the two-term sum representation,  $g(i, j) = \lambda_i + \lambda_j$ . We further set  $n_1 = n_2 = n_3 = n$ .

In the 3D case we consider the low-rank decomposition of the  $n \times n \times n$  reciprocal core tensor obtained by folding of the pseudo-inverse matrix  $\Lambda^+$ ,

$$\mathbf{G}^+ = [g_+(i, j, k)] \approx \left[ \frac{1}{g(i, j, k)} \right], \quad (4.9)$$

with entries defined for  $i, j, k = 1, \dots, n$ , by plugging zero value in the element  $g_+(1, 1, 1)$ , and leaving the rest of the elements in the reciprocal tensor  $[\frac{1}{g(i, j, k)}]$  unchanged,

$$g_+(1, 1, 1) = 0 \quad \text{and} \quad g_+(i, j, k) = \frac{1}{\lambda_i + \lambda_j + \lambda_k} \quad \text{otherwise.} \quad (4.10)$$

The theory on the low-rank tensor approximation of the target tensor  $\mathbf{G}^+$  is based on the integral Laplace transform representation of the discrete function  $g_+(i, j, k) = (\lambda_i + \lambda_j + \lambda_k)^{-1}$  for  $i + j + k > 3$

$$g_+(i, j, k) = \frac{1}{\pi} \int_0^\infty e^{-(\lambda_i + \lambda_j + \lambda_k)t} dt, \quad (4.11)$$

under the conditions

$$\lambda_i + \lambda_j + \lambda_k \geq a > 0, \quad i, j, k = 1, \dots, n, \quad \text{for} \quad i + j + k > 3, \quad (4.12)$$

which is satisfied for our construction.

Given  $\varepsilon > 0$ , under the condition (4.12) there exist the rank- $R$  canonical  $\varepsilon$ -approximation of the tensor  $\mathbf{U} = [\frac{1}{\lambda_i + \lambda_j + \lambda_k}]$  with  $R = O(|\log \varepsilon|)$ , see for example [24] for more details. Then we split the target tensor  $\mathbf{G}^+$  into the sum

$$\mathbf{G}^+ = \mathbf{G}_1 + \mathbf{G}_{m-1},$$

where

$$\mathbf{G}_1 = \mathbf{G}^+ \quad \text{for} \quad i = 1, j, k = 1, \dots, m, \quad \text{and} \quad \mathbf{G}_1 = 0 \quad \text{otherwise,}$$

while

$$\mathbf{G}_{n-1} = \mathbf{G}^+ - \mathbf{G}_1.$$

Now applying the result for tensors of the type  $\mathbf{U}$  to each of components separately we easily obtain the rank bounds

$$\text{rank}(\mathbf{G}_{n-1}) \leq R \quad \text{and} \quad \text{rank}(\mathbf{G}_1) \leq R + 1,$$

thus implying the desired upper bound on the canonical rank

$$\text{rank}(\mathbf{G}^+) \leq 2R + 1.$$

This argument proves the following

**Lemma 4.2** *Given  $\varepsilon > 0$ , under the condition (4.12) there exist the rank- $R$  canonical  $\varepsilon$ -approximation of the tensor  $[\frac{1}{\lambda_i + \lambda_j + \lambda_k}]$ . The target tensor  $\mathbf{G}^+$  can be approximated by a rank  $2R + 1$  canonical decomposition with accuracy  $2\varepsilon$ , where  $R = O(|\log \varepsilon|)$ .*

From the algorithmic point of view, the rank-structured approximation to the discrete periodic Laplacian inverse operators is performed by using the multigrid Tucker decomposition of the 3D tensors obtained by reshaping of the diagonal system matrix represented in the Fourier basis into a 3D tensor  $\mathbf{G}^+$ . The subsequent Tucker-to-canonical decomposition, see [23], transforms the Tucker core tensor to a canonical one with a small rank, preserving the approximation precision of the Tucker decomposition.

Now assume that  $\mathcal{F}(A)$  can be expressed approximately by a short-term linear combination of Kronecker rank-1 matrices. Then, the low-rank approximation of  $\mathcal{F}(A)$  is reduced to approximation of the diagonal matrix  $\mathcal{F}(A)$ . Assume we have a decomposition (in 2D case)

$$\mathcal{F}(A) = \sum_{k=1}^R \text{diag}(\mathbf{u}_1^{(k)} \otimes \mathbf{u}_2^{(k)}),$$

with vectors  $\mathbf{u}_i^{(k)} \in \mathbb{R}^{m_i}$  and  $R \ll \min(n_1, n_2)$ . Now let  $\mathbf{x} \in \mathbb{R}^{N_d}$  be a vector given in a low-rank format, i.e.

$$\mathbf{x} = \sum_{j=1}^S \mathbf{x}_1^{(j)} \otimes \mathbf{x}_2^{(j)},$$

with vectors  $\mathbf{x}_i^{(j)} \in \mathbb{R}^{n_i}$  and  $S \ll \min(n_1, n_2)$ . Then a matrix-vector product can be calculated by using only 1D matrix-vector operations

$$\begin{aligned} \mathcal{F}(A)\mathbf{x} &= (F_1^* \otimes F_2^*) \left( \sum_{k=1}^R \text{diag}(\mathbf{u}_1^{(k)} \otimes \mathbf{u}_2^{(k)}) \right) (F_1 \otimes F_2) \left( \sum_{j=1}^S \mathbf{x}_1^{(j)} \otimes \mathbf{x}_2^{(j)} \right) \\ &= (F_1^* \otimes F_2^*) \left( \sum_{k=1}^R \text{diag}(\mathbf{u}_1^{(k)} \otimes \mathbf{u}_2^{(k)}) \right) \left( \sum_{j=1}^S F_1 \mathbf{x}_1^{(j)} \otimes F_2 \mathbf{x}_2^{(j)} \right) \\ &= \sum_{k=1}^R \sum_{j=1}^S F_1^* (\mathbf{u}_1^{(k)} \odot F_1 \mathbf{x}_1^{(j)}) \otimes F_2^* (\mathbf{u}_2^{(k)} \odot F_2 \mathbf{x}_2^{(j)}), \end{aligned} \quad (4.13)$$

where  $\odot$  denotes the componentwise (Hadamard) product of 1D vectors. Using the FFT, the expression (4.13) can be computed in factored form in  $\mathcal{O}(RSn \log n)$  flops, where  $n = \max(n_1, n_2)$ .

In the case  $d = 3$ , equation (4.13) takes a form

$$\mathcal{F}(A)\mathbf{x} = \sum_{k=1}^R \sum_{j=1}^S F_1^* (\mathbf{u}_1^{(k)} \odot F_1 \mathbf{x}_1^{(j)}) \otimes F_2^* (\mathbf{u}_2^{(k)} \odot F_2 \mathbf{x}_2^{(j)}) \otimes F_3^* (\mathbf{u}_3^{(k)} \odot F_3 \mathbf{x}_3^{(j)}), \quad (4.14)$$

and similar in the general case of  $d > 3$ . Notice that the total number of terms in (4.14), that is  $RS$ , does not depend on the number of dimensions  $d$ .

The numerical performance of the PCG iteration with the rank-structured preconditioner  $A_{\Delta}^+$  described above will be discussed in section 5.

## 5 Numerical study

### 5.1 Fast solvers using matrix generation combined with tensor-product preconditioner

Here, we consider the beneficial properties of the presented elliptic problem solver applied to the case of checkerboard type coefficients profile compared with the previous scheme with more general overlapping-type configurations [22]. Figure 5.1 illustrates the configuration of the stochastic realization for checkerboard type coefficient with large RVE size,  $L = 256$ .

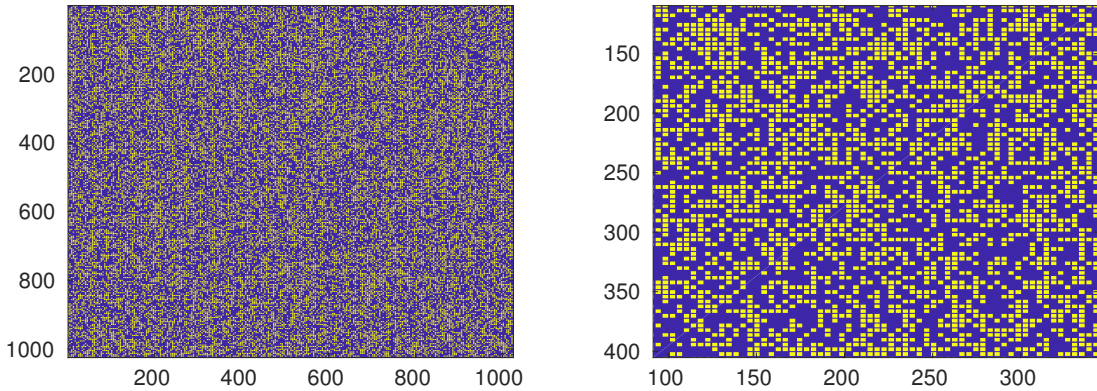


Figure 5.1: Example of the realization of coefficient for  $L \times L$  lattice with  $L = 256$ ,  $\alpha = 1/4$ , computed on the grid  $n \times n$  with  $n = 1024$ . Right panel zooms for the coefficients configuration on the left.

Table 5.1 compares the CPU times (sec.) for matrix generation, calculation of the loading vector in the right-hand side, and for the PCG iteration in the course of solving equation (4.1) for the general case of overlapping-type realizations of coefficients considered in [22] (marked by (1)), and for the approach presented in this paper and based on the low-rank preconditioner (marked by (2)). Here we set  $n_0 = 4$ ,  $\alpha = 1/4$  (see Figure 5.1, top), such that the vector size  $n_1$  on the finest grid is about  $n_1 \approx 4.0 \cdot 10^6$ . The iteration stopping criteria is chosen by  $\epsilon = 10^{-8}$ .

Solver (1) corresponding to overlapping coefficients profile displays limitations in the matrix generation times (dominating part in the calculations) for  $L = 128$ , which exceeds 561 seconds. Matrix generation time for the solver (2) using checkerboard-type coefficient is essentially smaller (1.4 seconds), which is important taking into account the required large number of realizations (up to  $M \sim 10^4 \div 10^5$ ) to be performed for analyzing important quantities of stochastic problem in random media. For larger  $L$  the solver (2) might be limited by the solution time, which is about 360 seconds for  $L = 512$ .

The latter limitation can be relaxed by using the low Kronecker rank (LKR) preconditioner  $A_{\Delta}^+$  described in the previous section. In this case we observe the balance between the matrix generation cost and that for the PCG iteration. Table 5.2 represents CPU times (sec.) for PCG iteration with a regularized preconditioner (RP)  $(-\Delta_h + \delta I)^{-1}$  and

$L^2$	$m/m^2$	matr. (1)	matr. (2)	RHS (1)	RHS (2)	solve (1)	solve (2)
$4^2$	17/289	0.012	0.006	0.01	0.007	0.006	0.01
$8^2$	33/1089	0.06	0.007	0.045	0.003	0.137	0.027
$16^2$	65/4225	0.34	0.014	0.19	0.010	0.11	0.15
$32^2$	129/16641	3.0	0.038	0.8	0.014	0.5	0.6
$64^2$	257/66049	36	0.24	3.7	0.069	2.6	2.2
$128^2$	513/263169	561	1.4	22	0.38	13.8	11.9
$256^2$	1025/ $1.0 \cdot 10^6$	–	11.3	–	2.84	–	66.8
$512^2$	2049/ $4.0 \cdot 10^6$	–	105.6	–	1.2	–	360.0

Table 5.1: CPU times (sec) for generating the stiffness matrix for the 2D stochastic homogenization problem, the right-hand side, and for the solution of the discretized linear system of equations for the checkerboard type realizations (2), compared with that for the case of overlapping samples (1).

with the LKR preconditioner by using the rank-structured approximation of the pseudo-inverse matrix  $A_{\Delta}^+$ , both applied with parameters  $n_0 = 4$ ,  $\alpha = 1/4$  and tolerance  $\epsilon = 10^{-8}$ . The number of inclusions varies from 16 to  $512^2$ .

$L^2$	$4^2$	$8^2$	$16^2$	$32^2$	$64^2$	$128^2$	$256^2$	$512^2$
RP	0.007	0.04	0.14	0.6	3.4	12.4	59.4	382.0
LKRP	0.008	0.02	0.02	0.8	0.27	0.9	6.1	11.0

Table 5.2: CPU times for PCG solver with a regularized preconditioner (RP) and with the rank-structured preconditioner (LKR),  $A_{\Delta}^+$ ,  $n_0 = 4$ ,  $\alpha = 1/4$ .

Figure 5.3 (left) visualizes the data presented in Tables 5.1 and 5.2.

Finally we notice that our numerical tests confirm Lemma 4.1 which proves uniform spectral equivalence of the preconditioned in both the grid-size  $n_1$  and the RVE size  $L$ . Indeed, fixed the stopping criteria, the number of PCG iterations was almost the same for numerical experiments in 2D and 3D cases.

## 5.2 Fast solver for the 3D stochastic problem

Numerical simulations for 3D stochastic homogenization require much larger computational resources compared with 2D case. Notice that fixed  $n_0 = 4$ , the problem size (i.e., vector size  $N_d = n^d$ ) in the 3D case for  $L = 32$  and  $L = 64$  equals to  $n^3 = 129^3$  and  $n^3 = 257^3$ , respectively, where  $n = n_0 L + 1$ . The assembling of the corresponding huge  $N_d \times N_d$  system matrix  $A$  is performed by fast tensor based techniques as described in section 3.3, see also [22]. The system matrix has to be recomputed for large number of stochastic realizations  $m = 1, \dots, M$ , that might be of the order of several tens of thousand and more.

Figure 5.2 (left) illustrates the configuration of the matrix coefficient visualized for the 3D realization on the  $L \times L \times L$  lattice, with  $L = 32$ ,  $n_0 = 8$  and the density parameter  $\alpha = 1/4$ . The number of inclusions is about  $\frac{1}{2}L^3 \approx 16000$ . Figure 5.2 (right) presents the example of random coefficient with two different values of contrast.

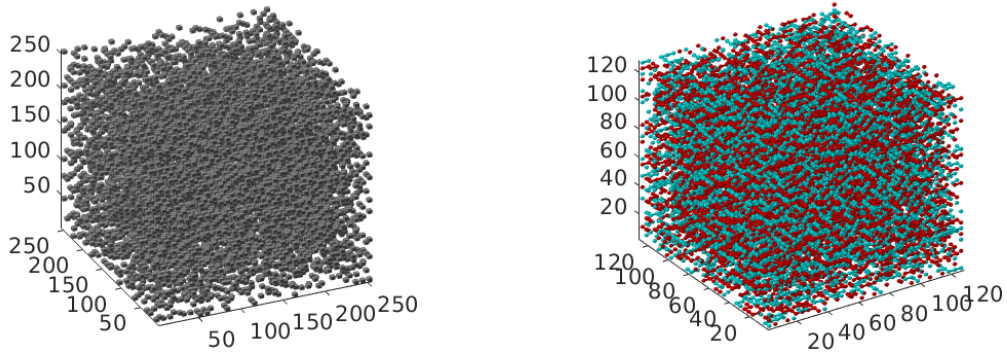


Figure 5.2: Example of 3D stochastic coefficient on  $L \times L \times L$  lattice with  $L = 32$  with fixed contrast coefficient (left) and the coefficient with two randomly distributed values of contrast.

$L^3$	$n_1/n_1^3$	$h$	$S$	matr.	RHS	solver
$4^3$	17/ 4913	6.25e-02	32	0.012	0.013	0.04
$8^3$	33/ 35937	3.13e-02	238	0.02	0.015	0.13
$16^3$	65/ 274625	1.56e-02	2048	0.1	0.05	0.62
$32^3$	129/ 2.1+06	7.81e-03	16338	2.4	0.38	11.2
$64^3$	257/ 16.9e+06	3.90e-03	131494	28.9	2.7	35.1
$128^3$	513/ 135e+06	1.95e-03	1049066	431.7	20.6	425

Table 5.3: CPU times (sec) for generating the stiffness matrix for the 3D stochastic homogenization problem, the right-hand side, and for the solution of the discretized linear system of equations. A vector size of the corresponding problem is  $n_1^3$ , and  $h$  is the mesh size.

We demonstrate the computational complexity of the robust iterative solver for 3D elliptic problems applying the stopping criteria  $\varepsilon = 10^{-7}$ . In all cases the number of PCG iterations did not exceed 20 uniformly in the problem size.

Table 5.3 displays the computation times for one solve of the 3D stochastic problem for increasing RVE size of  $L^3$ , and respectively increasing vector size  $n_1^3$  in the linear system of equations, as well as the number of stochastic samples,  $S$ , for the fixed realization. For example, the vector size for  $L = 128$  is about  $135 \cdot 10^6$ , and the corresponding number of stochastic samples exceeds  $10^6$ . This huge problem is solved in about 7 minutes (425 sec) in Matlab. Figure 5.3 (right) visualizes the data presented in Table 5.3.

We point out that the main time consuming steps include the matrix generation and the solution of the discrete elliptic problem for every of three dimensions by calling the “PCG” iteration routine with the rank-structured preconditioner in the form of periodic Laplacian pseudo inverse. We observe the well balanced complexity of both time consuming steps of the algorithms.

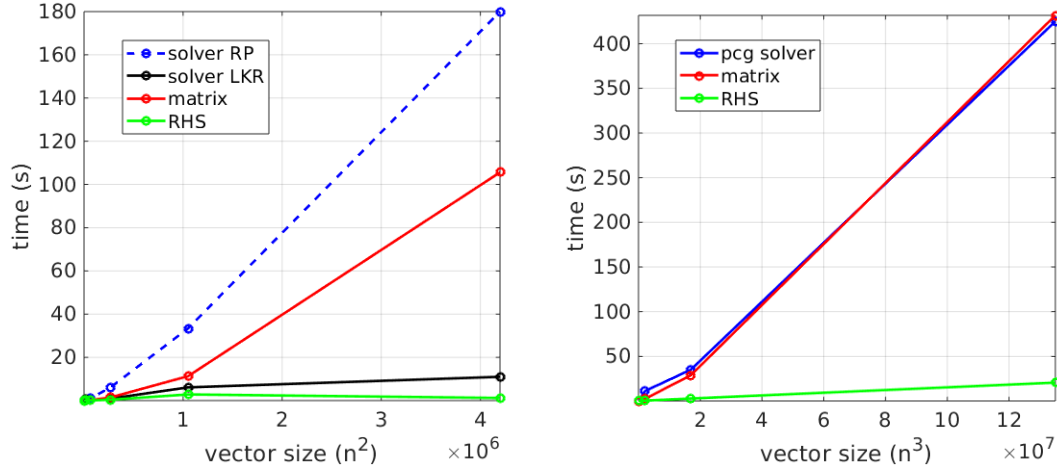


Figure 5.3: Left panel (2D case): times for matrix generation (red line), computation of the RHS (green) and for solution of the linear system by the regularized preconditioner (dashed blue) and by the tensor based LKR preconditioner (black) versus the 2D problem size  $n^2$ . Right panel (3D case): times for matrix generation (red line), computation of the RHS (green) and for solution of the 3D problem (blue) versus the system size  $n^3$ .

### 5.3 Example of application to numerical estimation of the homogenized coefficient matrix

The set of numerical approximations  $\{\bar{\mathbb{A}}_L^{(m)}\}$  to the homogenized matrix  $\mathbb{A}_{\text{hom}}$  is calculated by (3.16) for the sequence  $\{\mathbb{A}_L^{(m)}(x)\}$  of  $m = 1, \dots, M$  realizations, where  $M$  is large enough, and the artificial period  $L$  defines the size of RVE. For a fixed  $L$ , the approximation  $\bar{\mathbb{A}}_L^M$  is computed as the *empirical average* of the sequence  $\{\bar{\mathbb{A}}_L^{(m)}\}_{m=1}^M$ ,

$$\bar{\mathbb{A}}_L^M = \frac{1}{M} \sum_{m=1}^M \bar{\mathbb{A}}_L^{(m)}. \quad (5.1)$$

By the law of large numbers we have that the empirical average converges almost surely to the *ensemble average* (expectation)

$$\langle \bar{\mathbb{A}}_L \rangle_L = \lim_{M \rightarrow \infty} \bar{\mathbb{A}}_L^M. \quad (5.2)$$

Furthermore, by qualitative homogenization theory, as the artificial period  $L \rightarrow \infty$ , this converges to the homogenized matrix, see [16],

$$\mathbb{A}_{\text{hom}} := \lim_{L \rightarrow \infty} \langle \bar{\mathbb{A}}_L \rangle_L. \quad (5.3)$$

In some cases, we use the entry-wise notation for  $d \times d$  matrices  $\mathbb{A} = [a_{ij}]$ ,  $i, j = 1, \dots, d$ , for example,  $\langle \bar{\mathbb{A}}_L \rangle_L = [\bar{a}_{L,ij}]$  and  $\bar{\mathbb{A}}_L^{(m)} = [\bar{a}_{L,ij}^{(m)}]$ , etc.

As an example for application of our techniques, we numerically study the asymptotic of the *random part* of the error (standard deviation) for fixed  $N$  of moderate size, to confirm the theoretical convergence rate in  $L$ , see [16],

$$\sigma_L = \langle |\mathbb{A}_{\text{hom}} - \langle \bar{\mathbb{A}}_L \rangle_L|^2 \rangle_L^{1/2} \leq C L^{-d/2}. \quad (5.4)$$

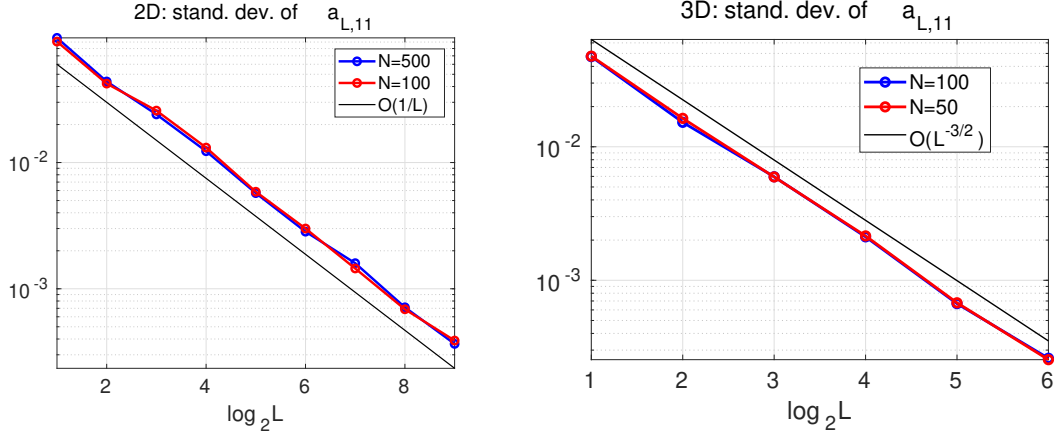


Figure 5.4: Standard deviation for 2D case  $a_{L,11}$  versus  $L$ ,  $N = 500$ ,  $L = 2^p$ ,  $p = 1, 2, \dots, 9$  (left) and for 3D case  $N = 100$ ,  $L = 2^p$ ,  $p = 1, 2, \dots, 6$  (right);  $n_0 = 4$ ,  $\alpha = \frac{1}{4}$ ,  $\lambda = 0.4$ .

In numerical experiments the theoretical value of standard deviation  $\sigma_L$  is approximated by the commonly used computable quantity  $\sigma_L^M$  calculated for a long enough sequence of  $M$  realizations by

$$\sigma_L^M = \sqrt{\frac{1}{M-1} \sum_{m=1}^M (\bar{\mathbb{A}}_L^{(m)} - \bar{\mathbb{A}}_L^M)^2}.$$

The numerical results are illustrated in Figure 5.4. The calculations for 2D case, depicted in the left panel can be compare with the similar results in [22] obtained for the case of overlapping coefficients sampling. Figure 5.4, right, confirms the asymptotic estimate in (5.4) for 3D case.

## 6 Conclusions

We present the numerical techniques for discretization and fast solution of the 2D and 3D elliptic equations with strongly varying piecewise constant coefficients arising in numerical analysis of stochastic homogenization problems for multi-scale composite materials. We use random checkerboard coefficient configurations with the large size of the RVE,  $L$ . For a fixed  $L$ , our method allows to avoid the generation of the new FEM space at each stochastic realization. For every realization, fast assembling of the FEM stiffness matrix is performed by agglomerating the Kronecker tensor products of 1D FEM discretization matrices.

The spectrally close preconditioner is constructed by using the low Kronecker rank approximation to the pseudo-inverse of discrete 2D and 3D periodic Laplacian. The resulting large linear system of equations is solved by the preconditioned CG iteration with the convergence rate that is independent of  $L$  and the grid size, as well as of the variation in jumping coefficients. The numerical tests illustrate the performance of the Matlab implementation in both 2D and 3D cases.

The proposed elliptic problem solver can be applied in the numerical analysis of 3D stochastic homogenization problems for ergodic processes with variable contrast in random

coefficients, for solving numerically the 3D stochastic elliptic PDEs in random heterogeneous materials, for solution of quasi-periodic (multi-scale) geometric homogenization problems, in the computer simulation of dynamical many body interaction processes and multi-particle electrostatics, as well as for numerical analysis of optimal control problems in random media.

### Acknowledgements

The authors are thankful to Prof. Felix Otto for useful discussions and motivation to develop an efficient solution scheme for the 3D elliptic PDEs with random coefficients in relation to numerical simulations for stochastic homogenization problems.

## References

- [1] G. Allaire. *Shape optimization by the homogenization method*. Springer Science & Business Media, Band 146, 2012.
- [2] A. Anantharaman, R. Costeaouec, C. Le Bris, F. Legoll and F. Thomines. *Introduction to numerical stochastic homogenization and the related computational challenges: some recent developments*. In Lecture Notes Series, Institute for Mathematical Sciences, Vol. 22, eds. Weizhu Bao and Qiang Du (National University of Singapore), 2011, pp 197–272.
- [3] A. Bensoussan, J.-L. Lions, and G. Papanicolaou. *Asymptotic Analysis for Periodic Structures*. American Mathematical Society, 1978.
- [4] E. Cances, V. Ehrlacher, F. Legoll, and B. Stamm. *An embedded corrector problem to approximate the homogenized coefficients of an elliptic equation*. C. R. Acad. Sci. Paris, Serie I, 353:801-806, 2015.
- [5] Eric Cances, Virginie Ehrlacher, Frederic Legoll, Benjamin Stamm, Shuyang Xiang. *An embedded corrector problem for homogenization. Part I: Theory*. E-preprint arXiv:1807.05131, 2018.
- [6] Eric Cances, Virginie Ehrlacher, Frederic Legoll, Benjamin Stamm, Shuyang Xiang. *An embedded corrector problem for homogenization. Part II: Algorithms and discretization*. arXiv: <http://arxiv.org/abs/1810.09885v1>, 2018.
- [7] A. Cohen, R. Devore, C. Schwab. *Analytic regularity and polynomial approximation of parametric and stochastic elliptic PDE's*. Analysis and Applications 9 (01), 11-47, 2011.
- [8] S. Dolgov, B. N. Khoromskij, A. Litvinenko, H. G. Matthies. *Polynomial chaos expansion of random coefficients and the solution of stochastic partial differential equations in the tensor train format*. SIAM/ASA Journal on Uncertainty Quantification 3 (1), 1109-1135, 2015.
- [9] S. Dolgov, R. Scheichl. *A Hybrid Alternating Least Squares–TT-Cross Algorithm for Parametric PDEs*. SIAM/ASA Journal on Uncertainty Quantification 7 (1), 260-291, 2019.
- [10] B. Engquist and P.E. Souganidis. *Asymptotic and numerical homogenization*. Acta Numerica, 17:147190, 2008.
- [11] Julian Fischer. *The choice of representative volumes in the approximation of the effective properties of random materials*. E-preprint, arXiv:1807.00834, 2018.
- [12] P. Frauenfelder, C. Schwab, R. A. Todor. *Finite elements for elliptic problems with stochastic coefficients*. Computer methods in applied mechanics and engineering 194 (2-5), 205-228, 2005.
- [13] A. Gloria and F. Otto. *An optimal variance estimate in stochastic homogenization of discrete elliptic equations*. Ann. Probab., 39:779856, 2011.



- [14] Antoine Gloria and Felix Otto: *An optimal error estimate in stochastic homogenization of discrete elliptic equations*. In: The annals of applied probability, 22 (2012) 1, p. 1-28.
- [15] Antoine Gloria and Felix Otto. *The corrector in stochastic homogenization: near-optimal rates with optimal stochastic integrability*. arXiv: <http://arxiv.org/abs/1510.08290>, 2016.
- [16] Antoine Gloria and Felix Otto. Quantitative estimates on the periodic approximation of the corrector in stochastic homogenization In: ESAIM / Proceedings, 48 (2015), p. 80-97. DOI: 10.1051/proc/201448003.
- [17] G. Heidel, V. Khoromskaia, B. Khoromskij, and V. Schulz. *Tensor approach to optimal control problems with fractional  $d$ -dimensional elliptic operator in constraints*. E-preprint, arXiv:1809.01971v2, 2018.
- [18] V. Jikov, S. Kozlov, and O. Oleinik. *Homogenization of differential operators and integral functionals*. Springer, Berlin, 1995.
- [19] T. Kanit, S. Forest, I. Galliet, V. Mounoury and D. Jeulin. *Determination of the size of the representative volume element for random composites: statistical and numerical approach*. Int. J. of Solids and Structures, 40, 2003, 3647-3679.
- [20] V. Kazeev, I. Oseledets, M. Rakhuba, C. Schwab. *Quantized tensor FEM for multiscale problems: diffusion problems in two and three dimensions*. E-preprint arXiv:2006.01455, 2020.
- [21] V. Khoromskaia and B. N. Khoromskij. *Tensor numerical methods in quantum chemistry*. De Gruyter, Berlin, 2018.
- [22] V. Khoromskaia, B. N. Khoromskij, and F. Otto. *Numerical study in stochastic homogenization for elliptic partial differential equations: Convergence rate in the size of representative volume elements*. Numer. Lin. Algebra Appl., 27 (3), e2296, 2020.
- [23] B. N. Khoromskij and V. Khoromskaia. *Multigrid Tensor Approximation of Function Related Arrays*. SIAM J. Sci. Comp., 31(4), 3002-3026 (2009).
- [24] Boris N. Khoromskij. *Tensor Numerical Methods in Scientific Computing*. Research monograph, De Gruyter Verlag, Berlin, 2018.
- [25] B.N. Khoromskij, and I. Oseledets. *Quantics-TT collocation approximation of parameter-dependent and stochastic elliptic PDEs*. Comp. Meth. in Applied Math., 10(4):34-365, 2010.
- [26] B.N. Khoromskij, A. Litvinenko, and H.G. Matthies. *Application of hierarchical matrices for computing the Karhunen-Loève expansion*. Computing **84**: 49-67 (2009).
- [27] B.N. Khoromskij and S. Repin. *Rank structured approximation method for quasi-periodic elliptic problems*. Comput. Methods in Appl. Math. 2017; 17 (3):457-477.
- [28] B. N. Khoromskij and Ch. Schwab. *Tensor-structured Galerkin approximation of parametric and stochastic elliptic PDEs*. SIAM J. Sci. Comput. 33 (1), 364-385, 2011.
- [29] S.M. Kozlov. *Averaging of random operators*. Matematicheskii Sbornik, 151(2):188-202, 1979.
- [30] F. Y. Kuo, C. Schwab, I. H. Sloan. *Quasi-Monte Carlo finite element methods for a class of elliptic partial differential equations with random coefficients*. SIAM Journal on Numerical Analysis 50 (6), 3351-3374, 2012.
- [31] C. Le Bris and F. Legoll. *Examples of computational approaches for elliptic possibly multiscale PDEs with random inputs*. J Comp. Phys., 328 (2017) 455-473.
- [32] B. Schmitt, B. Khoromskij, V. Khoromskaia, and V. Schulz. *Tensor Method for Optimal Control Problems Constrained by Fractional 3D Elliptic Operator with Variable Coefficients*. E-preprint, arXiv:2006.09314, 2020.
- [33] C. Schwab, C. J. Gittelsohn. *Sparse tensor discretizations of high-dimensional parametric and stochastic PDEs*. Acta Numerica 20, 291-467, 2011.